

Elastica Surface Generation of Curved-Crease Origami

Ting-Wei Lee^a, Zhong You^b, Joseph M. Gattas^{a,*}

^a*School of Civil Engineering, University of Queensland, St. Lucia, Australia*

^b*Department of Engineering Science, University of Oxford, Oxford, UK*

Abstract

Curved-crease origami are studied for many novel applications across engineering and architecture, as they are developable but possess a non-zero principal curvature and a corresponding energy storage capability when folded. However, geometric modelling techniques are limited, with most methods requiring numerical discretisation of a target curved surface to allow developability constraints to be enforced at vertices. The discretised surface can approximate a physical surface through relaxation for minimum bending energy, however such methods are cumbersome and their accuracy is largely unknown. This paper presents an analytical geometric construction method for curved-crease origami that avoids the need for surface discretisation. The new method combines a 1D elastica solution for large elastic bending deformation with a straight-crease origami projection and reflection process; it can thus concisely and accurately capture the principal surface curvature and developability characteristics of elastically-bent curved-crease origami. A surface error analysis of 3D scanned physical prototypes is used to validate the model, which is shown to be accurate to within $\pm 50\%$ of the sheet thickness for a 2mm thick model for a range of elastica surface profiles. Limitations of the model are also explored including the derivation of a maximum compressibility limit; investigation of accuracy of numerical folding motion simulation; and an investigation of a free edge distortion behaviour which occurs in certain origami forms.

Keywords: curved-crease origami, elastica, developable surface

*Corresponding author.

Email address: j.gattas@uq.edu.au (Joseph M. Gattas)

1. Introduction

Curved-crease origami geometries create 3D surfaces that are developable but contain regions with a non-zero principal curvature. This striking feature has led to the adoption of curved-crease forms for numerous novel engineering and architectural applications. These include compliant and lamina-emergent mechanisms [1, 2], self-assembling devices [3], energy-absorption components [4, 5], façade and shading components [6, 7], sculpture and artwork [8], and deployable and thin-walled structures [9, 10, 11, 12, 13, 14].

A range of geometric modelling techniques have been developed to realise these applications. By necessity, these all must capture two characteristics of curved-crease origami surfaces: enforcement of a constant zero Gaussian curvature for surface developability and evaluation of the non-zero principal curvature for surface bending behaviour. For simple curved surfaces such as ribbons, cylinders, and cones, developability is inherent and so the modelling technique need only evaluate the non-zero principal curvature with consideration of sheet bending stiffness [15] or elastic and kinetic energy [16]. For complex curved surfaces, developability is enforced with a vertex angle criterion, specifically that angles around each vertex sum to 2π [17, 18]. Complex curved surfaces are therefore typically numerically discretised to enforce vertex developability constraints, with the generated discrete developable surface [19] then approximating either an *exact* or *inexact* bending behaviour.

Inexact methods approximate an observed curved crease surface but are simplified to avoid explicit consideration of material bending behaviours. Examples include generation of an inexact surface through tracing of a physical prototype [20], progressive smoothing of a user-defined mesh [21], or curved-based and spline-based approximation of curved panels [22, 23, 24]. Exact methods combine geometric developability constraints with a consideration of material bending behaviours to give a notionally accurate representation of a curved crease surface. Examples include minimisation of bending energy on a specified straight-line ruling pattern [25] or a generated planar-quadrangle (PQ) mesh [26, 27].

The capacity of inexact or exact techniques for accurately capturing the non-zero principal curvature of curved-crease origami is largely unknown [28, 29], however early studies have suggested that the correspondence between designed and manufactured geometry is approximate only [30, 31]. There is also a prevalence of numerical modelling methods due to the need

to enforce developability as a vertex constraint. The few analytical modelling methods available are simple in that they model a complex curved surface by transformation of a simple curved surface, for example through mirror reflection [32] or tessellation [33].

This study describes a curved-crease origami analytical modelling method that avoids the need for surface discretisation and can therefore concisely and accurately capture developability and bending behaviours. The method uses a rigid-foldable origami base geometry as an initial developable design surface, from which a 1D elastica solution is extruded and reflected to give a curved-crease surface corresponding to a minimum elastic bending energy configuration. Section 2 describes the geometric construction method that combines the elastica, reflection, and straight-crease transformation processes. Section 3 examines the accuracy of the modelling method with 3D surface error analysis of manufactured prototypes. Section 4 combines the new analytical method with existing numerical approaches to capture the behaviour of several curved-crease geometries with different boundary conditions, followed by a discussion of future research implications in Section 5.

2. Curved-Crease Origami Creation

2.1. *Elastica Curves*

Elastica curves are geometries that describe the large elastic deformation of a slender beam [34]. Early mathematical models describe the elastica geometries as one-dimensional curves and were subsequently shown in mechanics models to represent naturally stable bending forms, that is curves corresponding to minimum bending energy configurations and also post-buckling geometries [35, 36, 37]. They have been extensively studied for a range of boundary conditions and deformations, with a typical elastica for a pinned-pinned beam with uniform bending stiffness shown Figure 1. The curve represents the centreline geometry of the deformed beam and possesses a non-uniform curvature, in contrast to the uniform curvature typically assumed for small beam deformations.

From structural mechanics, the relationship between beam curvature κ and deflection y is given by Equation 1. The non-linear denominator term arises from the large deformation strain-displacement relation, which includes finite rotation of a beam element. The constitutive relationship is unchanged

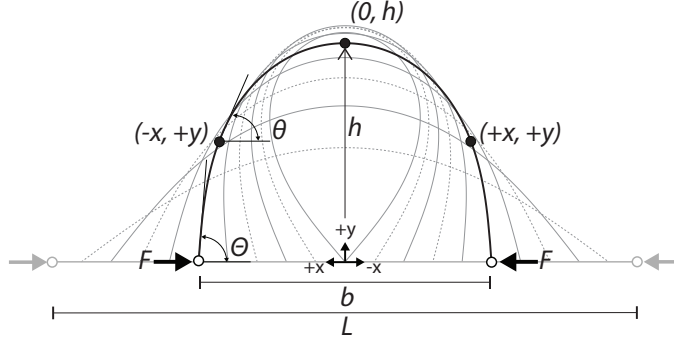


Figure 1: Elastica curves for a simply-support slender beam with uniform bending stiffness.

from linear theory, with curvature related to moment M and flexural rigidity value EI as shown.

$$\kappa = \frac{y''(x)}{\left(1 + y'(x)^2\right)^{\frac{3}{2}}} = \frac{M}{EI} \quad (1)$$

The elastica profile is obtained through integration of Equation 1, however retention of the denominator term makes this a complex task. The denominator term is usually neglected in engineering structures with assumed small beam deformations, however in large elastic deformation the term cannot be neglected. Mathematically, the solution for certain idealised cases can be achieved with Jacobian elliptic functions [38], however explicit solutions have also been derived, including for the case of one-dimensional simply-support beams. This paper shall employ the explicit solution developed by Pacheco et al. [39] and Valiente [40], which expresses the elastica curve in Cartesian coordinates and is published as a Visual Basic script online [41]. The solution is summarised as follows.

The 1D rod shown in Figure 1 has three length parameters: support distance after deformation b , beam height after deformation h , and beam length before deformation (arc length) L . These can be explicitly related to the m parameter, which is a quantity used to evaluate elliptic functions and generally employed such that $0 < m < 1$ [42]. Relations between the length and m parameters are [39]:

$$\frac{b}{L} = 2 \frac{E(m)}{K(m)} - 1 \quad (2)$$

92

$$\frac{h}{L} = \frac{\sqrt{m}}{K(m)} \quad (3)$$

93

$$\frac{b}{h} = \frac{2E(m) - K(m)}{m} \quad (4)$$

94 where $K(m)$ is the complete elliptic integral of the first kind and $E(m)$ is
 95 the complete elliptic integral of the second kind. The m parameter can be
 96 additionally related to the tangent angle of the elastica curve at the initial
 97 (pinned support) location Θ with [40]:

$$\Theta = 2 \sin^{-1} \left(\sqrt{m} \right) \quad (5)$$

98 A unique elastica curve can be defined in a Cartesian system $(\pm x, y)$ from
 99 Θ and m parameters. First, the vertical coordinate y and tangent angle θ are
 100 related with [40]:

$$y = \frac{0.5L\sqrt{2}\sqrt{\sin(\Theta - \frac{\pi}{2}) - \sin(\theta)}}{K(m)} \quad (6)$$

101 which can be rearranged as:

$$\theta = \sin^{-1} \left(\sin \left(\Theta - \frac{\pi}{2} \right) - \left(K(m) \frac{y}{0.5L\sqrt{2}} \right)^2 \right) \quad (7)$$

102 Second, by specifying a range from 0 to h for y coordinates in Equation 7,
 103 the rotation θ at each point coordinate is obtained. This is used to determine
 104 the corresponding $\pm x$ coordinates as:

$$\pm x = \sqrt{\frac{EI}{2F}} \int_{\theta}^{-\frac{\pi}{2}} \frac{\sin(\omega)}{\sqrt{\sin(\Theta - \frac{\pi}{2}) - \sin(\omega)}} d\omega \quad (8)$$

105 where F is the value of the two opposing horizontal end forces. F is obtained
 106 through equilibrium and by assuming a uniform beam flexural rigidity of EI
 107 [39]:

$$F = EI \left(2 \frac{K(m)}{L} \right)^2 \quad (9)$$

108 Finally, substituting Equation 9 into Equation 8, the term $\sqrt{\frac{EI}{2F}}$ can be re-
 109 placed with $\frac{0.5L}{\sqrt{2K(m)}}$. The flexural rigidity term EI is eliminated and the
 110 elastica coordinates $(\pm x, y)$ are given as a purely geometric relation [40]:

$$\pm x = \frac{0.5L}{\sqrt{2K(m)}} \int_{\theta}^{-\frac{\pi}{2}} \frac{\sin(\omega)}{\sqrt{\sin(\Theta - \frac{\pi}{2}) - \sin(\omega)}} d\omega \quad (10)$$

111 Therefore, by specifying any two of b , h , L , m , or Θ , the remaining three
 112 parameters can be obtained from Equations 2 to 5 and a corresponding plot
 113 of $(\pm x, y)$ for $0 \leq y \leq h$ is obtained by evaluating Equation 7 and Equation
 114 10.

115 2.2. *Elastica Curves and Non-Zero Principal Curvature of a 3D Surface*

116 While elastic deformation of a 1D beam into a 2D curve is well under-
 117 stood, predicting the elastic bending deformation of a 2D surface into into a
 118 3D form is an ongoing challenge and necessitates consideration of the prin-
 119 cipal curvatures of a surface. A developable surface has zero Gaussian curva-
 120 ture. As Gaussian curvature is the product of the principal curvatures, for a
 121 developable curved-crease origami surface, one principal curvature is always
 122 zero and the remaining principal curvature is non-zero. It is here proposed
 123 that the 2D elastica curve formulation of Equation 1 can be adopted as
 124 the non-zero principal curvature of a constrained class of elastically-bent 3D
 125 surfaces and, by extension, provide an analytical solution for curved-crease
 126 origami forms with developability and minimum elastic bending energy char-
 127 acteristics.

128 To illustrate the creation of a 3D form with an elastica non-zero principal
 129 curvature, first consider a unique 1D elastica curve with parameters b and
 130 h , shown in Figure 2a and obtained from Equations 7 and 10. If extruded,
 131 it forms a 3D shell which is both developable and possesses a minimum
 132 bending energy, shown in Figure 2b. A simple curved-crease origami form
 133 can be obtained from an extruded shell using the mirror reflection method,
 134 which truncates and reflects the shell about an intersecting cutting plane as
 135 shown in Figure 2c-d. If the inverted shell segment is assumed to possess
 136 the same curvature as the original shell, the 3D curved-crease origami form
 137 is both developable and possesses a minimum bending energy.

138 Designing a more complex curved-crease surface using the mirror reflec-
 139 tion method requires sequential specification of truncation planes and shell

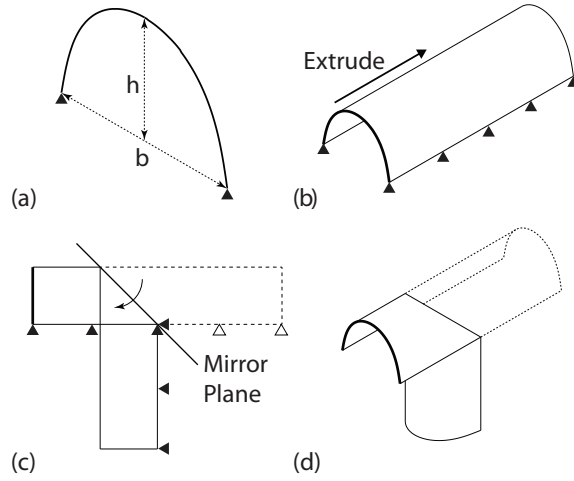


Figure 2: Creation of a 3D elastica surface. (a) 1D elastica curve with parameters b and h . (b) Extruded elastica curve demonstrates the deformed 3D shell. (c) Intersecting cutting plane on a 3D shell for mirror reflection. (d) Reflected 3D folded curved-crease component.

lengths. By reversing this process, that is by establishing reflection planes from a desired target volume, a direct method of surface design is achieved. This has been demonstrated previously by Gattas and You [22], with a ‘base’ rigid-foldable straight-crease origami pattern used to specify a target volume as shown in Figure 3a. Straight-crease patterns have folded volumetric parameter and unfolded (developable) parameter relationships that are easily established from vertex constraints. Reflection planes are also established at vertex crease locations, so by ‘projecting’ a curve along folded axes and reflecting about these planes, a developable surface with an inexact bending behaviour can be parametrised. Projection of an elliptical curve was shown to be sufficient for visual approximation of a curved-crease surface and simulation of surface folding via discretisation into a planar-quadrangle (PQ) mesh, shown in Figure 3b. If discrete rulings on the projected surface increase to infinity, a continuous developable curved-crease surface is parametrised, shown in Figure 3c. However the projected curve is inexact, that is it neglects bending energy considerations, and so the geometric construction remained an approximation only.

By combining the elastica surface projection shown in Figure 2 with the curved-crease surface design method shown in Figure 3, a geometric construc-

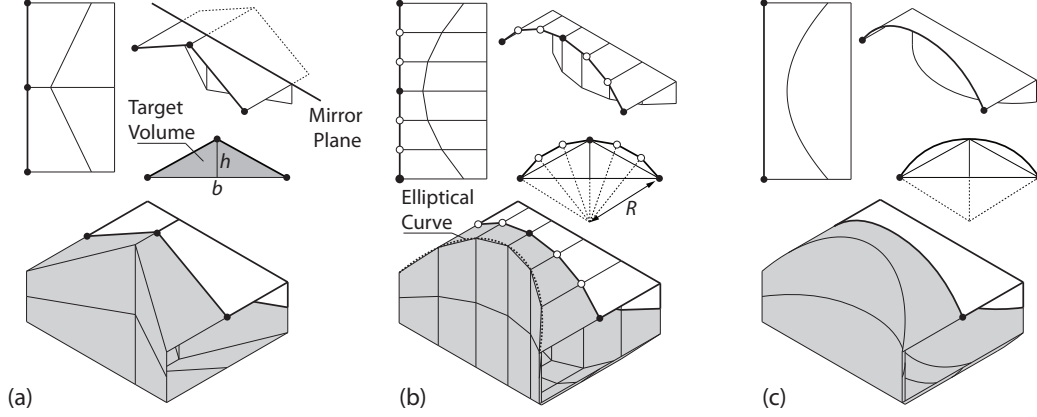


Figure 3: Parametrizations of (a) base rigid-foldable straight-crease origami geometry, (b) curved-crease surface approximated with PQ mesh, and (c) inexact curved-crease surface. Each sub-figure includes folded pattern, folded unit, unfolded unit, and 3D surface illustration.

tion method is achieved that concisely and accurately captures developability and bending behaviours. However, it includes a major assumption: the elastica remains a valid representation of the bending behaviour of the reflected surface. Key sub-assumptions are that the ‘crease line’ created from reflection about the truncation plane does not distort the bending behaviour of the surface; the free edges of the 3D shell do not distort the bending behaviour of the surface; and the surface edge boundary condition is preserved as pinned-pinned as per the original elastica derivation. These sub-assumptions will be systematically investigated in below sections.

2.3. Geometry Construction Method

A geometric construction method is developed here for projection of an elastica curve onto a target folded form. A base rigid-foldable configuration is shown in Figure 4a and is known as an ‘Arc’ pattern geometry. The unfolded configuration can be completely determined by three parameters: side lengths a_1 , b_1 , and sector angle ϕ . Remaining side length $a_2 = 2b_1 \cos(\phi) + a_1$, where $a_1 < a_2$. However, the primary interest is converting a single vertex geometry into its corresponding curved-crease form with minimum elastic bending energy. Therefore, the rectangular ‘transformation region’ is determined by side lengths c_1, c_2 , and d_1 , where $c_1 = a_1/2$, $c_2 = a_2/2$, and

178 $d_1 = b_1 \sin(\phi)$. The edge angles η_A and η_Z are useful in defining a particular
 179 folded configuration as shown in Figure 4b. The folded configuration then
 180 provides a target volume for designing an elastica curve, where the design
 181 parameters b and h are defined as:

$$b = 2b_1 \sin\left(\frac{\eta_z}{2}\right) \quad (11)$$

182

$$h = \sqrt{\left(d_1\right)^2 - \left(0.5b\right)^2} \quad (12)$$

183 As base pattern parameters are sufficient to define two of five elastica pa-
 184 rameters, a unique elastica curve exists for the target state. When projected
 185 as an assumed non-zero principal curvature along the folded transformation
 186 region, a curved-crease surface is created as shown in Figure 4c.

187 Continued projection of the elastica about all reflection planes, that is
 188 planes passing through all zig-zag base pattern edges, creates a complete
 189 curved-crease pattern as shown in Figure 4d. If all truncations are mapped
 190 to the original elastica extrusion, it can be seen that the Arc base pattern
 191 and curved crease pattern correspond to a linear elastica extrusion, that is
 192 a surface with free edges parallel to the elastica construction plane. The
 193 curved-crease Arc surface thus preserves all of the assumptions made in the
 194 previous section when adopting a 1D elastica curve to generate an linearly-
 195 extruded surface with non-zero principal curvature. Other straight-crease
 196 origami base patterns and their curved-crease variants can also be created
 197 with this method, however they possess varied free edge conditions that will
 198 affect the elastica curve validity. These will be explored in Section 4.

199 2.4. *Contact Limit State*

200 A related problem to that of exact bending behaviour is that of the com-
 201 pressibility limit of curved-crease origami surfaces. Several definitions for
 202 compressibility limit exist in literature, but in the context of elastic bending,
 203 it is defined here as the state at which adjacent curved panels are first in
 204 ‘contact’ during folding.

205

206 By using the method proposed in this paper, an analytical relationship
 207 can be derived for a ‘contact limit state’ which occurs when the initial ro-
 208 tation Θ of the elastica curve boundary edge is $\pi/2$. Beyond this point, a

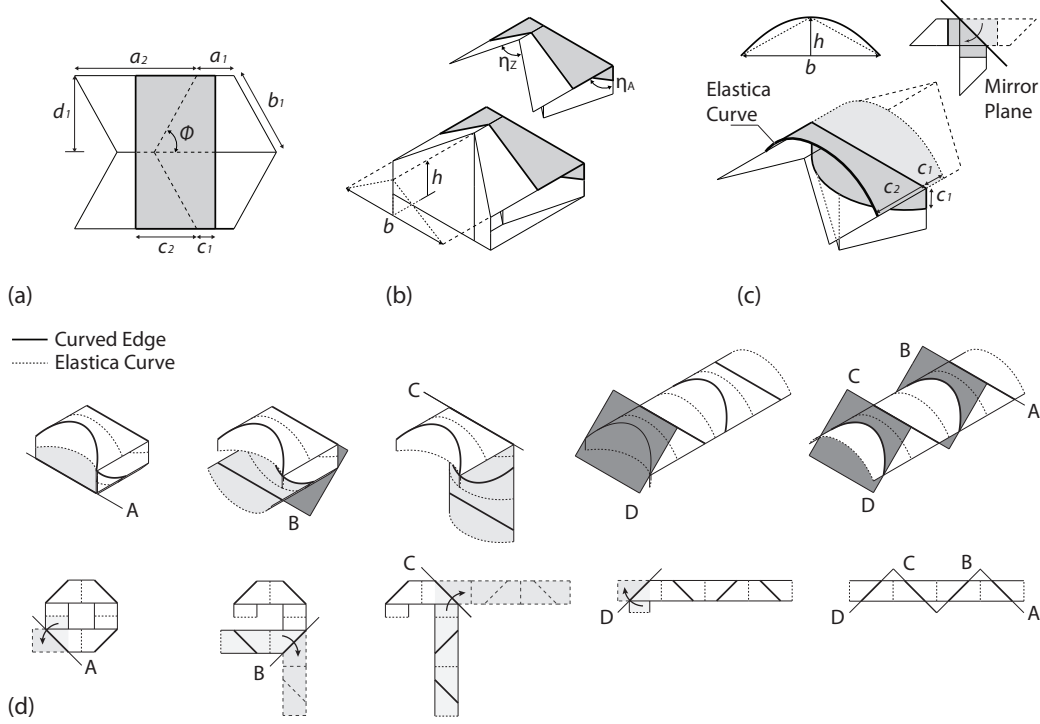


Figure 4: Geometry construction procedures for target folded curved-crease origami. (a) Unfolded base pattern, (b) folded base pattern and design parameters relevant for elastica curve specification, (c) elastica curve projected along transformation region to generate surface with exact non-zero principal curvature, (d) continuous projection of the elastica about all reflection planes and correspondence to linear elastica extrusion.

209 surface generated from the projection of the elastica curve will have contact-
 210 ing adjacent curved panels. From Equation 5, an upper limit of $\Theta = \pi/2$
 211 will limit the m parameter from 0 to 0.5. Figure 5 plots Equation 4 and it
 212 can be seen that a minimum b/h ratio of 1.1981 must exist for a non-con-
 213 tacting elastica curve with $m < 0.5$ to be constructable from straight-crease
 214 base pattern. It is noted that this is only a theoretical limit for elastic bend-
 215 ing. It is likely the system could be compressed further after contact occurs,
 216 although whether this causes plastic deformation of the constituent panels,
 217 reversible elastic deformation, and/or a change of the crease line location
 218 and configuration would depend on the material and manufacturing method

219 utilised in practice.

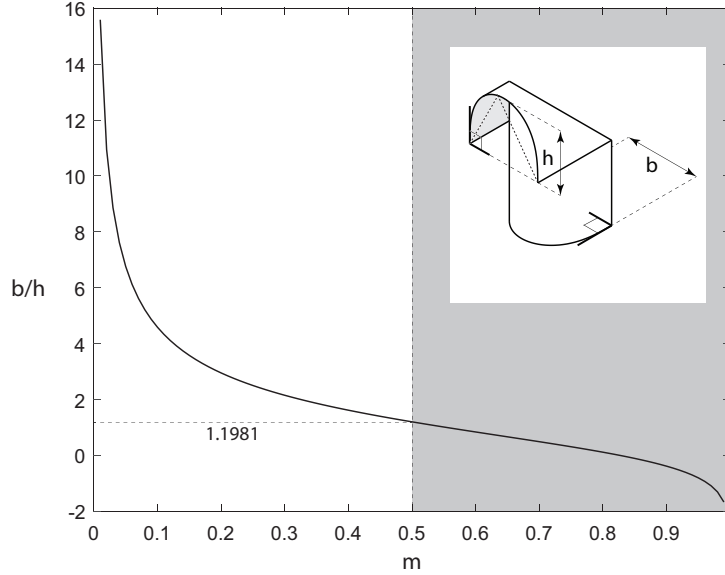


Figure 5: Curved-crease contact limit state. The shaded region indicates the curved-crease design parameters which would cause contact between adjacent curved panels.

220 3. Experimental Analysis

221 3.1. Method

222 To validate the hypothesised curved-crease elastica formulation, proto-
 223 types were manufactured and assessed for surface variance. All prototypes
 224 were manufactured with a 2.0mm thick isotropic polycarbonate sheet, with
 225 panels cut separately and joined with a fabric hinge. The sheet material
 226 achieved the necessary large elastic deformations during folding and the hinge
 227 material was selected as one with approximately zero rotational stiffness but
 228 with sufficient connectivity and stress transfer to resist the translation dis-
 229 placements and separation of parts during folding.

230 A series of prototypes were constructed to systematically explore the as-
 231 sumptions of constructing a 3D folded surface from a 1D elastica curve.
 232 For all prototypes, a pinned-pinned boundary condition is obtained with a
 233 manufactured jig to enforce a fixed boundary width b . Prototypes were then

234 3D scanned with a FaroArm 3D scan system. The collected mesh data was
 235 imported into a Rhino CAD environment and the surface error was measured
 236 between the scanned mesh and an ‘exact’ CAD geometry that incorporated
 237 a thickness offset from centreline geometry. A optimisation routine was used
 238 to align mesh and geometry, with the Galapagos optimisation solver used to
 239 move design geometry along 6-DOF rigid body displacements until a mini-
 240 mum surface error configuration was obtained.

241 The entire process is shown first for a simple 500mm \times 500mm sheet,
 242 deformed to a width of 350mm as shown in Figure 6a. A correspond-
 243 ing design surface was generated from an elastica curve with parameters
 244 $b/L = 350/500 = 0.7$ and extruded along a length of 500mm as shown in
 245 Figure 6b. The prototype is scanned and the mesh imported and aligned
 246 for minimum surface error as shown in Figure 6c. The design surface is
 247 then sampled with approximately ten thousand data extraction points and
 248 the error calculated as the distance between each design surface point and
 249 the closest point on the scanned surface. Error is displayed in Figure 6d as a
 250 coloured line between design and scanned points, with a colour legend from
 251 green to red for 0 to $+2t$ error and green to blue 0 to $-2t$ error, where $t = 2\text{mm}$.
 252 Red and blue regions therefore correspond to scanned surface points that lie
 253 above and below the simulated surface, respectively, and clear regions corre-
 254 spond to scanned surface points with line lengths approaching zero, that is
 255 regions approaching zero error. The overall accuracy of the surface is assessed
 256 with an average absolute surface error. This value was calculated as 0.78mm
 257 for the current prototype or just under 40% of sheet thickness, which shows
 258 the elastica design surface gives a highly accurate prediction of the scanned
 259 surface. The majority of error is seen to arise from scanning irregularities
 260 that occur at the pinned boundary.

261 3.2. *Single-Crease Reflection*

262 An initial set of prototypes was constructed to explore the exactitude and
 263 validity of a single truncation and reflection of the elastica extrusion, that
 264 is a single-crease reflection. One prototype was manufactured with from an
 265 elastica curve with design parameter $b/L = 0.75$. A second prototype was
 266 manufactured with the simplified method proposed by Gattas and You [22],
 267 which assumes an inexact curvature, here taken as uniform. Both forms are
 268 folded from a 400mm long rectangular sheet, and share design parameters b
 269 and h to achieve a common target design volume.

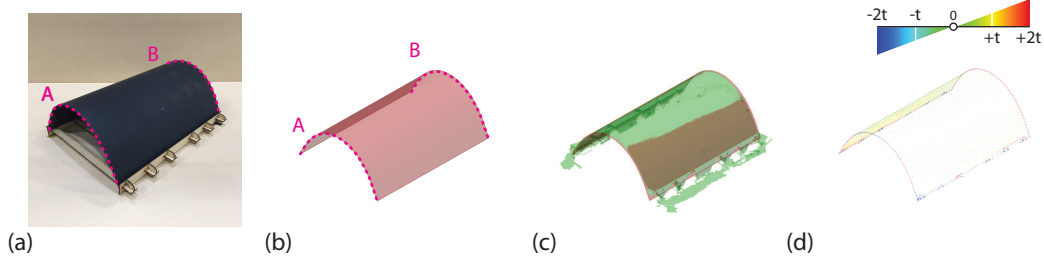


Figure 6: Surface error measurement of a simple deformed sheet, where $b/L = 0.7$. (a) Physical prototype, (b) simulated surface, (c) best-fit scanned surface, and (d) surface error result.

270 The elastica prototype and surface error is shown in Figure 7a and has
 271 an average absolute surface error of 0.88mm, extracted from approximately
 272 twenty thousand data points. This accuracy is similar to the non-reflected
 273 extrusion and confirms that reflection about the crease line does not distort
 274 the bending behaviour. The pinned boundary and free edge conditions are
 275 maintained and again are the main source of scanning error.

276 The simplified prototype and surface error is shown in Figure 7b and
 277 has an average absolute surface difference of 2.9mm, extracted from approx-
 278 imately twenty thousand data points. Interestingly, the minimum surface
 279 error occurs near the crease-line region, which implies the crease reflection
 280 and enforced developability constraint are able to somewhat enforce the as-
 281 sumed curvature. However away from the crease line, the uniform curvature
 282 assumption is seen to give a poor approximation of the manufactured surface.
 283 Looking at a cross-sectional comparison between manufactured and simpli-
 284 fied free-edge profiles in Figure 7c, it can be seen that the free edges tend to
 285 relax toward an elastica-like minimum bending energy state.

286 3.3. Constructed State

287 To examine the accuracy of the geometric construction method, selected
 288 geometries are designed and manufactured as shown in Figure 8a-c. Each de-
 289 sign is a four-sided tubular geometry corresponding to a constructed curved-
 290 crease Arc pattern. They are folded from a 1000mm \times 500mm rectangular
 291 sheet with elastica curve design parameters of $b/L = 0.75$, 0.85, and 0.95.

292 The surface error of each model was analysed with approximately twenty-
 293 four thousand data extraction points, with results shown in Figure 9. An

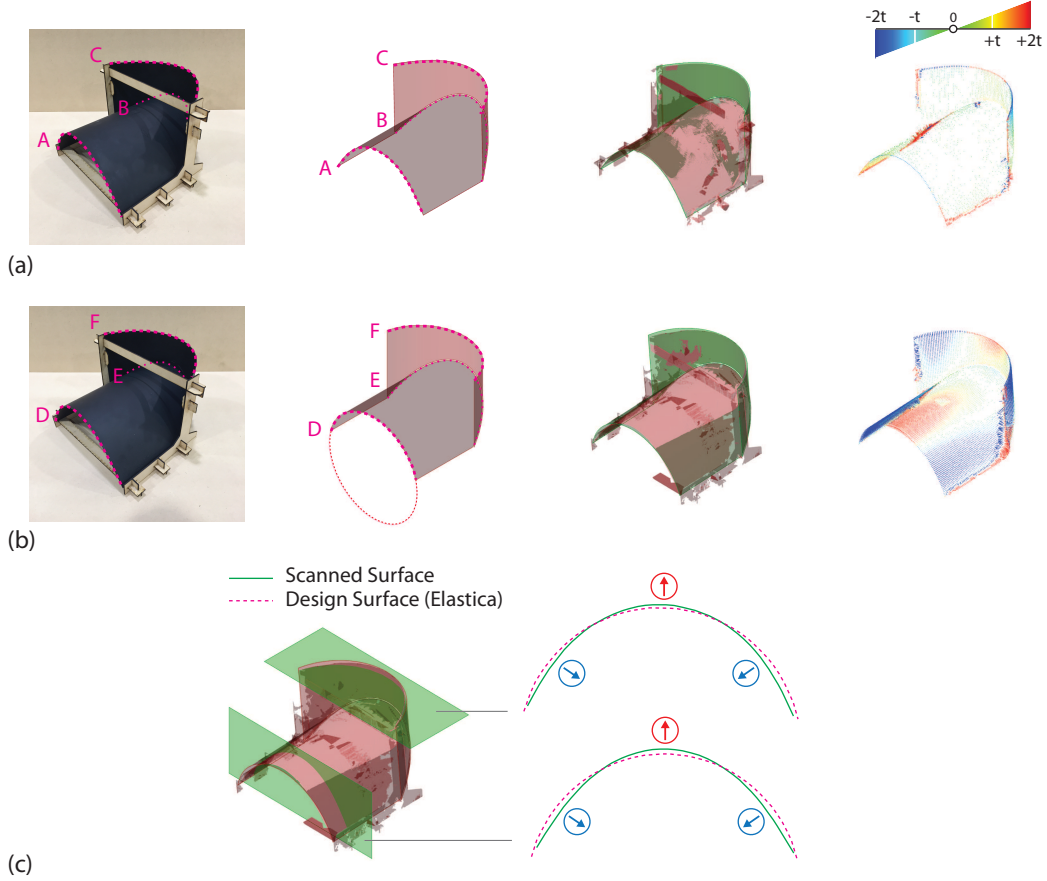


Figure 7: Single-crease reflection of surfaces with (a) exact elastica and (b) inexact (uniform) non-zero principal curvature. From left to right, unfolded planar pattern, simulated folded surface, best-fit scanned surface, and surface error result. (c) Cross section analysis.

294 average absolute surface error of 0.76mm, 0.64mm, 0.63mm was seen for
 295 $b/L = 0.75, 0.85, \text{ and } 0.95$, respectively. The correspondence demonstrates
 296 a high degree of design accuracy in terms of 3D surface prediction across a
 297 range of elastica profiles, with all average absolute surface differences within
 298 half of the 2mm sheet thickness. Regions of maximum and minimum sur-
 299 face error are seen around the boundary region and crease line, attributed
 300 primarily to manufacture and assembly defects. The higher errors in steeper
 301 elastica design curves are attributed to the same, with curved-crease pro-
 302 totypes with steeper non-zero principal curvatures being more difficult to

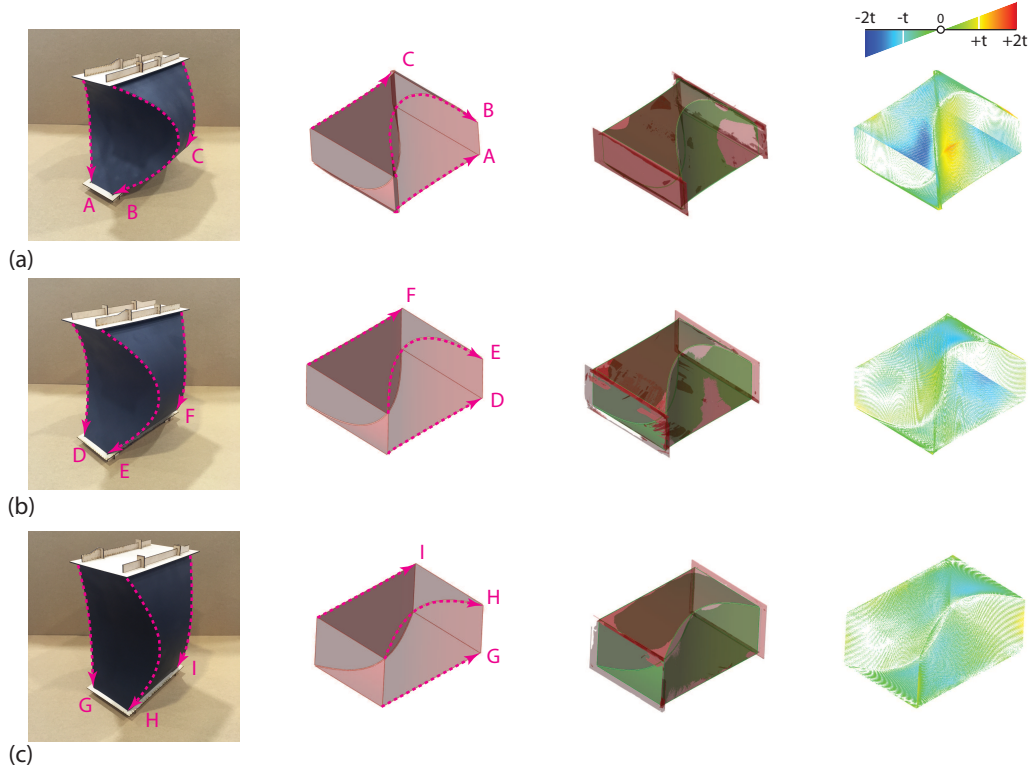


Figure 8: Surface error measurement of constructed state geometries. with elastica curve design parameter b/L of (a) 0.75, (b) 0.85, and (c) 0.95. From left to right, physical prototype, simulated surface, best-fit scanned surface, and surface error measurement result.

303 manufacture and assemble.

304 3.4. Surface Tessellation

305 The elastica curves used in previous examples are obtained by utilising
 306 a pinned-pinned elastica curve. Higher order elastica curves can be obtained
 307 [43], however their physical manifestation is highly dependant on restraint
 308 conditions. For example, the second mode elastica shape shown in Figure
 309 10a-b is an unstable elastic equilibrium state and one would expect the shape
 310 to return back to a first mode configuration. It is theorised though that
 311 for folded elastica surfaces, crease lines would provide a means by which to

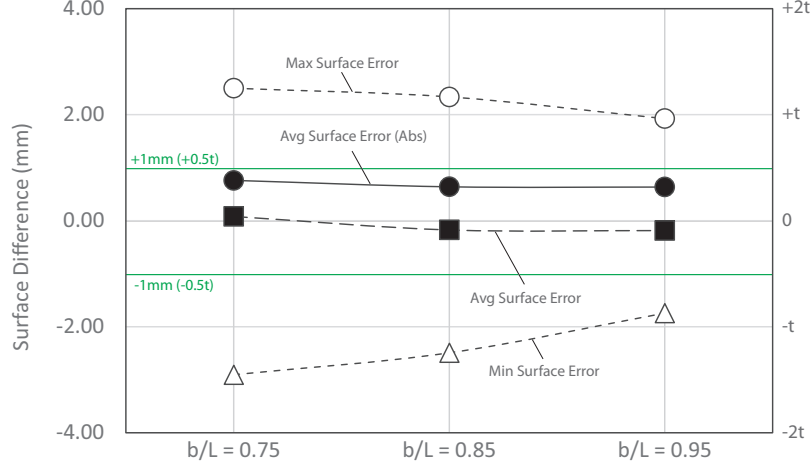


Figure 9: Constructed state surface error measurement results.

312 stabilise second or higher mode elastica curves, that is to say that once a
 313 higher-order crease line is generated with mirror reflection as shown in Fig-
 314 ure 10c, it would prevent a transition back to a lower mode as would be
 315 expected in the 1D case. A geometric construction is shown in Figure 10d
 316 for a curved-crease Arc pattern that utilises a second-mode elastica curve
 317 for generation of the 3D curved surface.

318 To measure the validity of adopting a second-mode elastica curve as the
 319 non-zero principal curvature for a folded surface, a prototype was manufac-
 320 tured from a 1000mm \times 800mm sheet and with $b/L = 0.9$, shown in Figure
 321 11. Surface error measurement was taken from approximately twenty-four
 322 thousand data extraction points and showed an average absolute surface dif-
 323 ference of 0.66mm, with errors again primarily occurring at the boundary and
 324 crease line regions due to manufacture and assembly defects. This high corre-
 325 spondence shows the second-mode elastica curve can be validly assumed as a
 326 non-zero principal curvature and mirror reflection can be utilised to stabilise
 327 and enable manifestation of higher mode minimum bending energy surfaces.

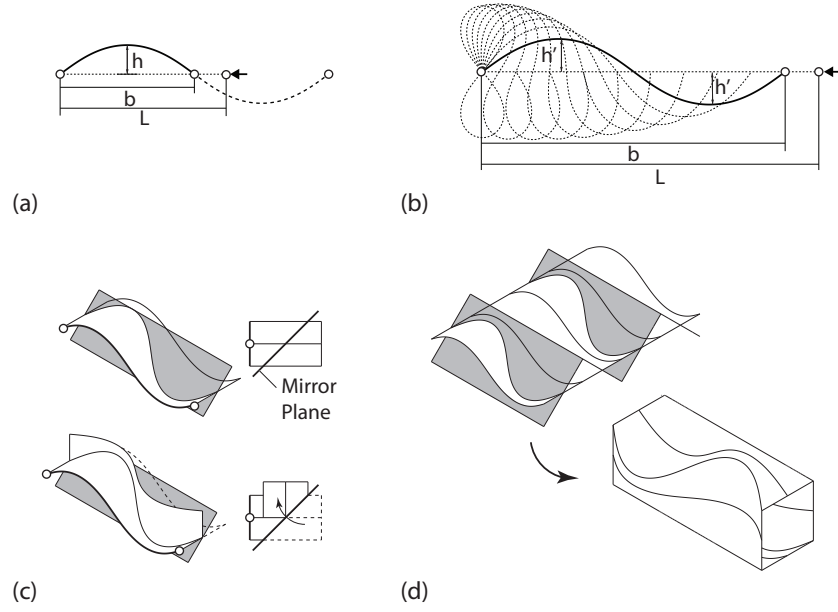


Figure 10: Design procedures of a curved-crease Arc pattern generated with a second-mode elastica curve. (a) First and second mode elastica curve, (b) second-mode elastica geometries, (c) folded unit, and (d) geometric construction.

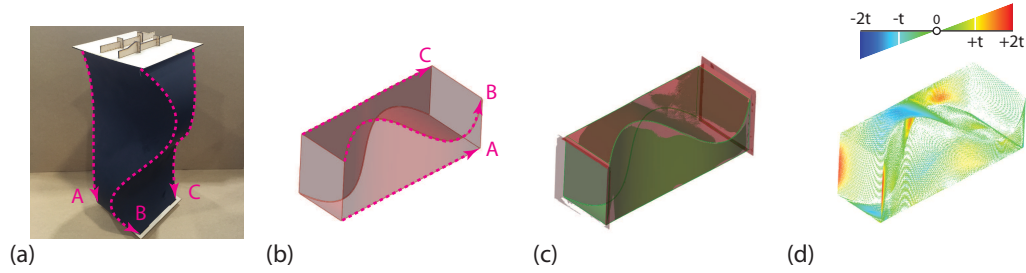


Figure 11: Surface error measurement of second-mode elastica surface. (a) Physical prototype, (b) simulated surface, (c) best-fit scanned surface, (d) surface error measurement result illustration.

328 4. Combined Numerical-Elastica Formulations

329 4.1. Folding Sequence

330 The elastica curve has been demonstrated to give a valid solution for non-
 331 zero principal curvature of a specific target folded state. However, in origami-

inspired engineering, it is often useful to simulate intermediate folded states, that is the folding sequence of a particular crease pattern. The elastica surface generation method cannot be used to generate valid intermediate states as the reflection planes used to generate a developability condition and the boundary parameters used to generate the elastica curve are only coincident in the target state. However, many numerical methods exist to simulate the folding behaviour of a known curved-crease surface and so an investigation was conducted to assess the extent to which a numerical folding simulation was able to accurately model the intermediate folded states of an elastica generated origami surface.

To simulate a folding sequence, a curved-crease origami pattern is constructed with a ‘Miura’ base pattern and elastica curve as shown in Figure 12a-b. The constructed surface is discretised into planar quadrangle strips to give a rigid-foldable piecewise assembly of straight-crease origami that approximates the generated elastica form, shown in Figure 12c. The folding motion of the piecewise assembly can then be simply simulated by numerically varying a common edge angle η_A [44], as shown in Figure 12d. Increasing the number of discrete rulings gives a stronger approximation of the initial target design surface, with a fold simulation consisting of quasi-infinite rulings shown in Figure 12e. This method is selected for investigation as it is a computationally inexpensive and highly inexact; component panels are made planar and no rotational stiffness is imparted to crease lines created during discretisation, so no bending behaviour energy exists in the system.

For practicality of testing, a physical prototype was constructed with two curved-crease Miura units joined together about a mirror plane as shown in Figure 12d-e. Each unit was folded from a 500mm \times 500mm sheet with elastica curve design parameters of $b/L = 0.7$. The prototype was scanned at four intermediate folded states, at an edge angle $\eta_A = 160^\circ, 140^\circ, 120^\circ, 100^\circ$, and at the target state with $\eta_A = 90^\circ$.

The surface error of each folded state was analysed with approximately twenty-four thousand data extraction points as shown in Figure 13, with results plotted in Figure 14. Errors are seen to increase in progressive states, with an average absolute surface error of 0.50mm, 0.48mm, 0.69mm, 0.94mm, 1.27mm seen for $\eta_A = 160^\circ, 140^\circ, 120^\circ, 100^\circ, 90^\circ$, respectively. The first three intermediate states show good correspondence between the numerical model and physical prototype, with the majority of errors seen around boundary regions in a similar manner to previous surface comparisons. This shows that numerical simulations can provide a good prediction of the surface geome-

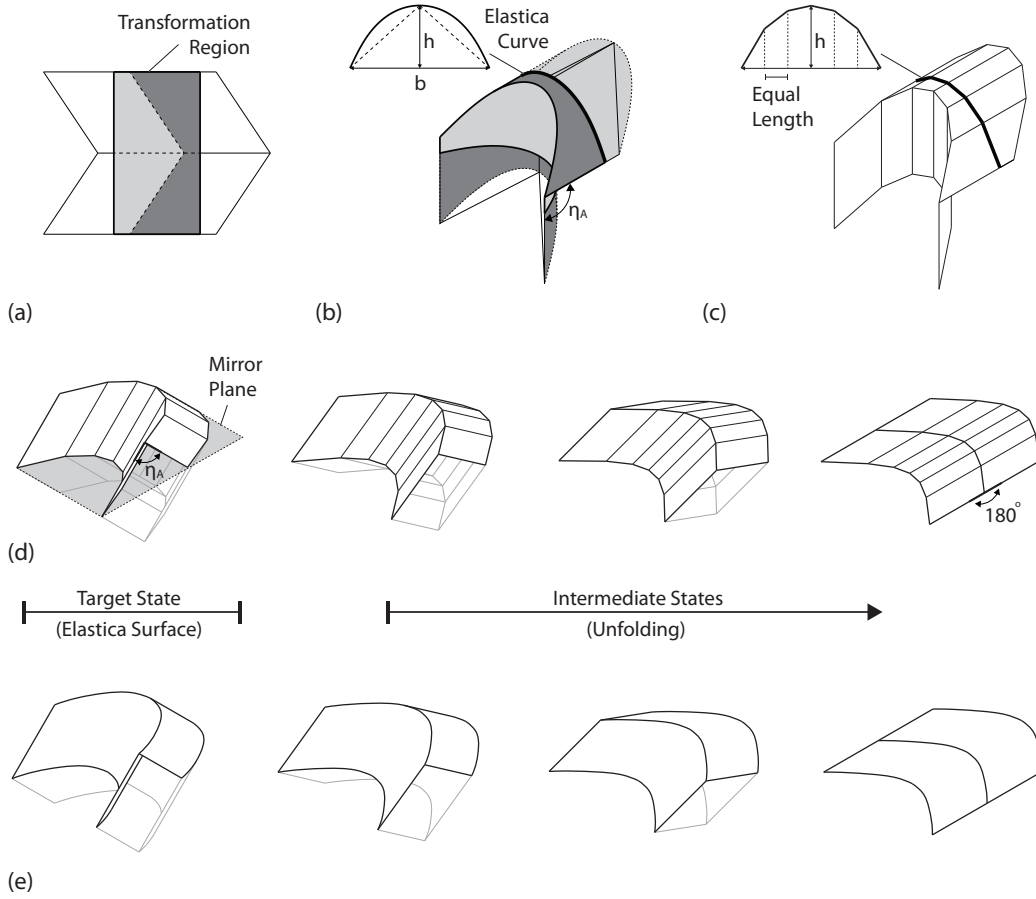


Figure 12: Numerical simulation of folding sequence of elastica generated surface. (a) Base unfolded Miura pattern, (b) curved-crease transformation, (c) rigid-foldable approximation of curved-crease surface, (d) numerical simulation of folding sequence of the rigid-foldable assembly, and (e) numerical simulation of folding sequence of a quasi-infinite rigid-foldable assembly.

try of intermediate folded states, even when simplified to neglecting bending energy considerations.

-Errors are seen to jump in the fourth intermediate state and the final target state, with the latter having an error that exceeds half of 2mm material thickness. Inspection of the error location shows it occurred at the connected edges of the Miura units, highlighted in Figure 13e. The primary source of

error was initially thought to be from manufacturing defects occurring due to the increased difficulty of attaching a fabric hinge to these non-developable edges. However, closer inspection suggested that the non-zero principal curvature of the surface no longer corresponded to the assumed analytical elastica curve in these edge regions. A final study was conducted to investigate this behaviour, described in the next section.

4.2. Free Edge Effect

For curved-crease models studied in Sections 2 and 3, the constructed elastica surfaces corresponded exactly to a linear extrusion of a 1D elastica solution, that is the ends, or ‘free edges’, lay in a plane parallel to the elastica construction plane. It was therefore assumed that the free edges of the 3D shell did not distort the bending behaviour of the elastica surface. However, this assumption is thought to be invalid for elastica surfaces generated on the Miura surface of the previous section, or for other base patterns which possess a non-parallel free edge. To explore the effect of the free edge, two elastica surface geometries were generated on a base pattern with non-parallel free edges.

The first investigated surface consists of the component panels of the curved-crease Miura pattern described in the previous section, shown in Figure 15a. These surfaces can be understood as a linear elastica extrusion with free edges that lie in parallel planes that are inclined or ‘skewed’ relative to the elastica construction plane, as shown in Figure 15b. The surface error measurement result shown in Figure 16a demonstrates a surface variation, with a flatter profile on the skew edge inclined towards the surface centreline and a steeper profile on the skew edge inclined away from the centreline. This variation is shown more clearly with a cross-sectional comparison in Figure 16b. To verify the error lay in the elastica assumption and not the prototype measurement, a numerical finite element simulation was also created to compare with the physical prototype. Results of this comparison are shown in Figure 17 and it can be seen that the numerical and physical behaviours have a much better correspondence. Average absolute surface error was 3.37mm for the elastica surface comparison and only 0.78mm for the numerical surface comparison, which shows the elastica curve is an invalid representation of non-zero principal surface curvature in skewed edge regions of 3D surfaces. It also confirms the free edge distortion is the likely cause of the error observed in the previous section.

412 A second surface was investigated to understand the effect of free edge dis-
 413 tortion in a reflected curved-crease origami surface. A single-crease model was
 414 constructed from an Arc-Miura base pattern, with skew edges and geometric
 415 construction procedure as shown in Figure 18a-b, respectively. Prototype
 416 parameters were for a 400mm long arc length, an extrusion length of 400mm,
 417 and an elastica curve design parameter of $b/L = 0.75$. The surface error
 418 measurement result is shown in Figure 19a and demonstrates a reasonable
 419 correspondence between the design and prototype surfaces, with an average
 420 absolute surface error of 1.1mm. Similar to that seen previously for the in-
 421 exact uniform curvature model, low error is seen in the crease line region,
 422 with the crease acting to enforce the assumed elastica principal curvature.
 423 Larger errors of up to approximately 3.1mm are seen towards the skewed
 424 free edge, shown more clearly in cross section in Figure 19b. A numerical
 425 finite element simulation was again used to check accuracy of the physical
 426 prototype, however a hybrid surface generation approach was used whereby
 427 a rectangular sheet was numerically deformed to the target width and then
 428 geometrically reflected about a plane, shown in Figure 20. This prevented
 429 an assumed crease line from altering the minimum bending energy config-
 430 uration. The average absolute surface error decreased to 0.98mm and the
 431 accuracy of the surface is seen to have improved both at crease line and free
 432 edge locations, shown with cross section profiles in Figure 20c.

433 5. Discussion

434 The investigations into curved-crease geometries constructed from ex-
 435 truded elastica curves showed that the proposed surface generation method
 436 is accurate if boundary conditions between the assumed 1D elastica solution
 437 and 3D curved-crease origami surface are consistent. This paper has only
 438 utilised a pinned-pinned elastica curve with a constant flexural rigidity EI ,
 439 which was shown to validly construct various curved-crease surfaces for both
 440 first and second mode elastica profiles. A range of elastica solutions exist
 441 for other boundary conditions, including fixed-fixed, fixed-pinned, and fixed-
 442 free conditions and for incorporation of axial and shear deformation terms
 443 within the elliptic integral [45] or non-uniform flexural rigidity caused by cross
 444 section (I) or material (E) variation [46, 47]. Recent studies have also made
 445 early investigations into the folding behaviour of origami patterns with elas-
 446 tically-deformed crease line regions [48, 49]. Utilisation of these elastica and

447 elastic folding solutions with the geometric construction method proposed in
448 this paper can potentially further improve accuracy and extend the range of
449 curved-crease origami geometries which can be specified analytically. Further
450 study is needed to develop this.

451 The free edge effect was seen to distort bending behaviour if the free edge
452 was not parallel to the elastica construction plane. This was demonstrated
453 for both linearly-extruded elastica surfaces and 3D reflected curved-crease
454 origami surfaces. The impact of this distortion on the validity of the con-
455 structed surface depends on the geometry under consideration. If the free
456 edge inclination is small in comparison to the extruded surface length, it
457 would be expected to have a minimal, localised impact as shown with Fig-
458 ure 19. It is also hypothesised that developable tubular origami geometries,
459 which effectively remove free edges, would avoid distortion completely. This
460 was the case for the single developable tubular geometry explored in this
461 paper, however further geometries of this type need to be studied to confirm
462 this hypothesis. In addition to distortion caused by free edge effects, study
463 of surface distortions arising from transitions between non-uniform crease
464 lines, introduction of interior vertices, or introduction of conical surface re-
465 gions could also lead to new insights and extend the range of curved-crease
466 origami geometries that can be specified.

467 Finally, a substantial limitation of the presented method is that a straight-
468 crease base pattern needs to be known *a priori* to generate the required
469 reflection planes and elastica design parameters. Whilst extensive families
470 of straight-crease patterns are known and accessible, the method is funda-
471 mentally unsuited to generative forms of origami-inspired engineering design
472 where an approximate straight-crease origami geometry is as-yet unknown or
473 where the precise final design state is unconstrained or not of primary inter-
474 est. However, the method is highly suitable for parametric forms of origami-
475 inspired engineering design, as an explicit relationship between crease pattern
476 parameters (for example as required for manufacture) and volumetric param-
477 eters of the design state (for example as required for 3D surface modelling
478 and engineering analysis) can be established relatively simply in a simpli-
479 fied straight-crease form and then ‘converted’ to an accurate curved-crease
480 form which may have a higher performative capacity. The combination of
481 generative and parametric design systems is an as-yet unexplored topic in
482 origami-inspired design.

483 6. Conclusion

484 This study has presented an analytical geometric construction method
485 for curved-crease origami that concisely and accurately captures curvature
486 and developability constraints. Developability is preserved without the need
487 for surface discretisation by projection and reflection of an assumed 2D elas-
488 tica profile about a known 3D straight-crease origami surface. The use of
489 an elastica curve for non-zero principal surface curvature gives a near-ex-
490 act analytical representation of 3D curved-crease origami surfaces that are
491 elastically-bent and have boundary conditions consistent with the utilised
492 elastica solution. Extensions of the method were explored and included iden-
493 tification of the compressibility limit of curved-crease surfaces; construction
494 of stable curved-crease origami surfaces from higher-order elastica profiles;
495 and demonstration that a numerical simulation of the folding motion of a
496 discretised curved-crease surface gave a good prediction of behaviour of a
497 physical prototype over a full range of motion.

498 Key limitations of the method are in modelling of surfaces which possess
499 free edge regions that are not parallel to the elastica construction plane and
500 the need to use of a straight-crease base pattern that approximates the de-
501 sired curved-crease form. Numerous further avenues for research are sug-
502 gested to overcome these limitations and extend the new method presented
503 here, including closer study of curvature transitions in curved-crease pat-
504 terns of different types and investigation of hybrid generative and parametric
505 origami design systems.

506 7. Acknowledgments

507 The authors gratefully acknowledge the financial support provided by the
508 Australian Research Council Discovery Project DP160103279.

- 509 [1] T. G. Nelson, R. J. Lang, S. P. Magleby, L. L. Howell, Curved-folding-
510 inspired deployable compliant rolling-contact element (d-core), *Mechan-*
511 *ism and Machine Theory* 96 (2016) 225–238.
- 512 [2] T. G. Nelson, R. J. Lang, N. A. Pehrson, S. P. Magleby, L. L. Howell,
513 Facilitating deployable mechanisms and structures via developable lam-
514 ina emergent arrays, *Journal of Mechanisms and Robotics* 8 (3) (2016)
515 031006.

- 516 [3] S. Miyashita, I. DiDio, I. Ananthabhotla, B. An, C. Sung, S. Arabagi,
517 D. Rus, Folding angle regulation by curved crease design for self-
518 assembling origami propellers, *Journal of Mechanisms and Robotics*
519 7 (2) (2015) 021013.
- 520 [4] J. Gattas, Z. You, The behaviour of curved-crease foldcores under low-
521 velocity impact loads, *International Journal of Solids and Structures* 53
522 (2015) 80–91.
- 523 [5] D. Garrett, Z. You, J. M. Gattas, Curved crease tube structures as an
524 energy absorbing crash box, in: *ASME 2016 International Design Engi-
525 neering Technical Conferences and Computers and Information in En-
526 gineering Conference*, American Society of Mechanical Engineers, 2016,
527 pp. V05BT07A017–V05BT07A017.
- 528 [6] A. Vergauwen, L. Alegria Mira, K. Roovers, N. De Temmerman, Para-
529 metric design of adaptive shading elements based on curved-line folding,
530 in: *Proceedings of the First Conference Transformables 2013*, 2013.
- 531 [7] G. Epps, S. Verma, Curved folding: Design to fabrication process of
532 robofold, in: *Shape Modeling International*, Bournemouth, UK, July,
533 2013, pp. 75–83.
- 534 [8] E. Demaine, M. Demaine, D. Koschitz, Reconstructing david huffmans
535 legacy in curved-crease folding, *Origami* 5 (2011) 39–52.
- 536 [9] J. P. Duncan, J. Duncan, Folded developables, in: *Proceedings of the
537 Royal Society of London A: Mathematical, Physical and Engineering
538 Sciences*, Vol. 383, The Royal Society, 1982, pp. 191–205.
- 539 [10] T. Tachi, Composite rigid-foldable curved origami structure, in: *1st In-
540 ternational Conference on Transformable Architecture (Transformables
541 2013)*, Seville, Spain, Sept, 2013, pp. 18–20.
- 542 [11] J. Lienhard, Bending-active structures: form-finding strategies using
543 elastic deformation in static and kinetic systems and the structural po-
544 tentials therein, 2014.
- 545 [12] B. Hansen, J. Tan, J. Gattas, D. Fernando, M. Heitzmann, Folded fab-
546 rication of frp-timber thin-walled beams with novel non-uniform cross-
547 sections, in: *World Conference on Timber Engineering*, Vienna Univer-
548 sity of Technology, 2016.

- 549 [13] J. T. Bruton, T. G. Nelson, T. K. Zimmerman, J. D. Fernelius, S. P.
550 Magleby, L. L. Howell, Packing and deploying soft origami to and from
551 cylindrical volumes with application to automotive airbags, Royal Soci-
552 ety open science 3 (9) (2016) 160429.
- 553 [14] M. G. Walker, K. A. Seffen, Bistable behaviour of creased thin metallic
554 strips, in: Proceedings of the IASS Annual Symposium 2017 "Interfaces:
555 architecture, engineering, science", International Association for Shell
556 and Spatial Structures (IASS), 2017.
- 557 [15] H.-D. Hwang, S.-H. Yoon, Constructing developable surfaces by wrap-
558 ping cones and cylinders, Computer-Aided Design 58 (2015) 230–235.
- 559 [16] Z. Shen, J. Huang, W. Chen, H. Bao, Geometrically exact simulation
560 of inextensible ribbon, in: Computer Graphics Forum, Vol. 34, Wiley
561 Online Library, 2015, pp. 145–154.
- 562 [17] D. A. Huffman, Curvature and creases: A primer on paper, IEEE Trans.
563 Computers 25 (10) (1976) 1010–1019.
- 564 [18] T. Tachi, Generalization of rigid foldable quadrilateral mesh origami, in:
565 Symposium of the International Association for Shell and Spatial Struc-
566 tures (50th. 2009. Valencia). Evolution and Trends in Design, Analysis
567 and Construction of Shell and Spatial Structures: Proceedings, Editorial
568 Universitat Politècnica de València, 2009.
- 569 [19] Y. L. Kergosien, H. Gotoda, T. L. Kunii, Bending and creasing virtual
570 paper, IEEE Computer graphics and applications 14 (1) (1994) 40–48.
- 571 [20] T. Tachi, G. Epps, Designing one-dof mechanisms for architecture by
572 rationalizing curved folding, in: International Symposium on Algorith-
573 mic Design for Architecture and Urban Design (ALGODE-AIJ). Tokyo,
574 2011.
- 575 [21] S. Bhooshan, Interactive design of curved-crease-folding, Ph.D. thesis,
576 University of Bath (2016).
- 577 [22] J. M. Gattas, Z. You, Miura-base rigid origami: parametrizations of
578 curved-crease geometries, Journal of Mechanical Design 136 (12) (2014)
579 121404.

- 580 [23] E. A. P. Hernandez, D. J. Hartl, D. C. Lagoudas, Kinematics of origami
581 structures with smooth folds, *Journal of Mechanisms and Robotics* 8 (6)
582 (2016) 061019.
- 583 [24] C. Tang, P. Bo, J. Wallner, H. Pottmann, Interactive design of devel-
584 opable surfaces, *ACM Transactions on Graphics (TOG)* 35 (2) (2016)
585 12.
- 586 [25] J. Solomon, E. Vouga, M. Wardetzky, E. Grinspun, Flexible developable
587 surfaces, in: *Computer Graphics Forum*, Vol. 31, Wiley Online Library,
588 2012, pp. 1567–1576.
- 589 [26] Y. Liu, H. Pottmann, J. Wallner, Y.-L. Yang, W. Wang, Geometric
590 modeling with conical meshes and developable surfaces, in: *ACM Trans-
591 actions on Graphics (TOG)*, Vol. 25, ACM, 2006, pp. 681–689.
- 592 [27] M. Kilian, S. Flöry, Z. Chen, N. J. Mitra, A. Sheffer, H. Pottmann,
593 Curved folding, in: *ACM Transactions on Graphics (TOG)*, Vol. 27,
594 ACM, 2008, p. 75.
- 595 [28] D. Koschitz, E. D. Demaine, M. L. Demaine, Curved crease origami,
596 *Advances in Architectural Geometry* (2008) 29–32.
- 597 [29] M. A. Dias, L. H. Dudte, L. Mahadevan, C. D. Santangelo, Geometric
598 mechanics of curved crease origami, *Physical review letters* 109 (11)
599 (2012) 114301.
- 600 [30] A. Vergauwen, L. De Laet, N. De Temmerman, Computational mod-
601 elling methods for pliable structures based on curved-line folding,
602 *Computer-Aided Design* 83 (2017) 51–63.
- 603 [31] T. Lee, J. Gattas, Folded fabrication of composite curved-crease com-
604 ponents, in: *8th International Conference on Fibre-Reinforced Polymer
605 (FRP) Composites in Civil Engineering (CICE 2016)*, 2016.
- 606 [32] J. Mitani, T. Igarashi, Interactive design of planar curved folding by re-
607 flection, in: *Pacific Conference on Computer Graphics and Applications-
608 Short Papers*, Kaohsiung, Taiwan, September, 2011, pp. 21–23.

- [33] S. Chandra, A. Körner, A. Koronaki, R. Spiteri, R. Amin, S. Kowli, M. Weinstock, Computing curved-folded tessellations through straight-folding approximation, in: Proceedings of the Symposium on Simulation for Architecture & Urban Design, Society for Computer Simulation International, 2015, pp. 152–159.
- [34] L. Euler, Methodus inveniendi lineas curvas maxima minimive proprietate gaudentes additamentum i, De Curvis Elasticis, Lausanne and Geneva 1744.
- [35] J. V. Huddleston, Nonlinear buckling and snap-over of a two-member frame, International Journal of Solids and Structures 3 (6) (1967) 1023–1030.
- [36] B. K. Horn, The curve of least energy, ACM Transactions on Mathematical Software (TOMS) 9 (4) (1983) 441–460.
- [37] C. L. Dym, I. H. Shames, et al., Solid mechanics, Springer, 1973.
- [38] T. Yang, Matrix displacement solution to elastica problems of beams and frames, International Journal of Solids and Structures 9 (7) (1973) 829–842.
- [39] Q. Pacheco, E. Piña, et al., The elastic rod, Revista mexicana de física E 53 (2) (2007) 186–190.
- [40] A. Valiente, An experiment in nonlinear beam theory, American journal of physics 72 (8) (2004) 1008–1012.
- [41] W. McElwain, A script for elastic bending (aka the elastica curve)<http://www.grasshopper3d.com/forum/topics/a-script-for-elastic-bending-aka-the-elastica-curve>
- [42] P. F. Byrd, M. D. Friedman, Handbook of elliptic integrals for engineers and physicists, Vol. 67, Springer, 2013.
- [43] V. G. A. Goss, The history of the planar elastica: insights into mechanics and scientific method, Science & Education 18 (8) (2009) 1057–1082.
- [44] J. M. Gattas, W. Wu, Z. You, Miura-base rigid origami: parameterizations of first-level derivative and piecewise geometries, Journal of mechanical design 135 (11) (2013) 111011.

- 639 [45] G. Yoshiaki, Y. Tomoo, O. Makoto, Elliptic integral solutions of plane
640 elastica with axial and shear deformations, International Journal of
641 Solids and Structures 26 (4) (1990) 375–390.
- 642 [46] B. K. Lee, J. F. Wilson, S. J. Oh, Elastica of cantilevered beams
643 with variable cross sections, International Journal of Non-Linear
644 Mechanics 28 (5) (1993) 579 – 589. doi:[http://dx.doi.org/10.1016/0020-](http://dx.doi.org/10.1016/0020-7462(93)90049-Q)
645 7462(93)90049-Q.
646 URL <http://www.sciencedirect.com/science/article/pii/002074629390049Q>
- 647 [47] B. K. Lee, S.-J. Oh, Elastica and buckling load of simple tapered
648 columns with constant volume, International Journal of Solids and
649 Structures 37 (18) (2000) 2507–2518.
- 650 [48] E. A. P. Hernandez, D. J. Hartl, E. Akleman, D. C. Lagoudas, Modeling
651 and analysis of origami structures with smooth folds, Computer-Aided
652 Design 78 (2016) 93–106.
- 653 [49] G. Secheli, A. Viquerat, G. S. Aglietti, A model of packaging folds in
654 thin metal-polymer laminates, Journal of Applied Mechanics 84 (10)
655 (2017) 101005.



Figure 13: Surface error measurement of numerical folding simulation. From left to right: physical prototype, simulated surface, best-fit scanned surface, and surface error measurement. Folded states generated with an the edge angle η_A of (a) 160° , (b) 140° , (c) 120° , (d) 100° , and (e) target state 90° .

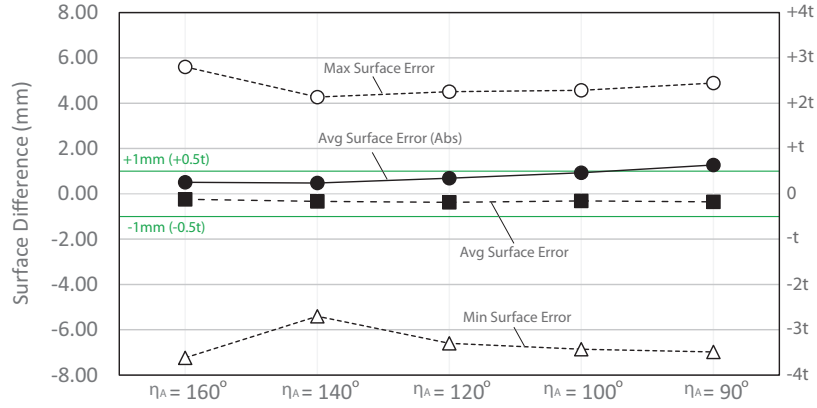


Figure 14: Folded state surface error measurement results.

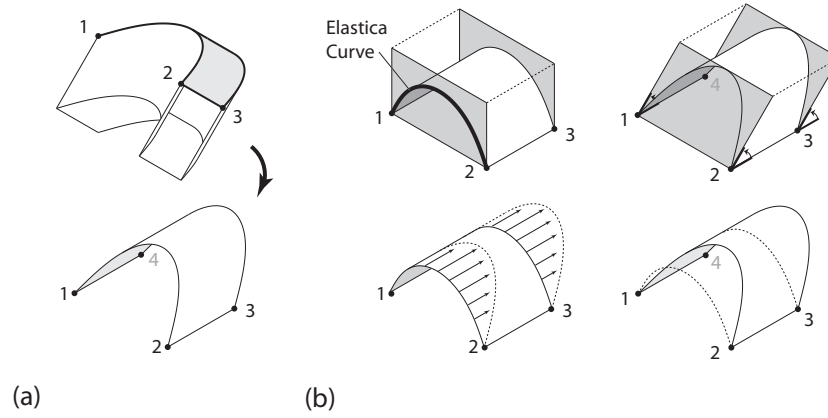


Figure 15: Surface geometry with skewed free edges. (a) Curved-crease Miura pattern geometry and (b) corresponding linear elastica curve extrusion with skewed edges lying in parallel inclined planes.

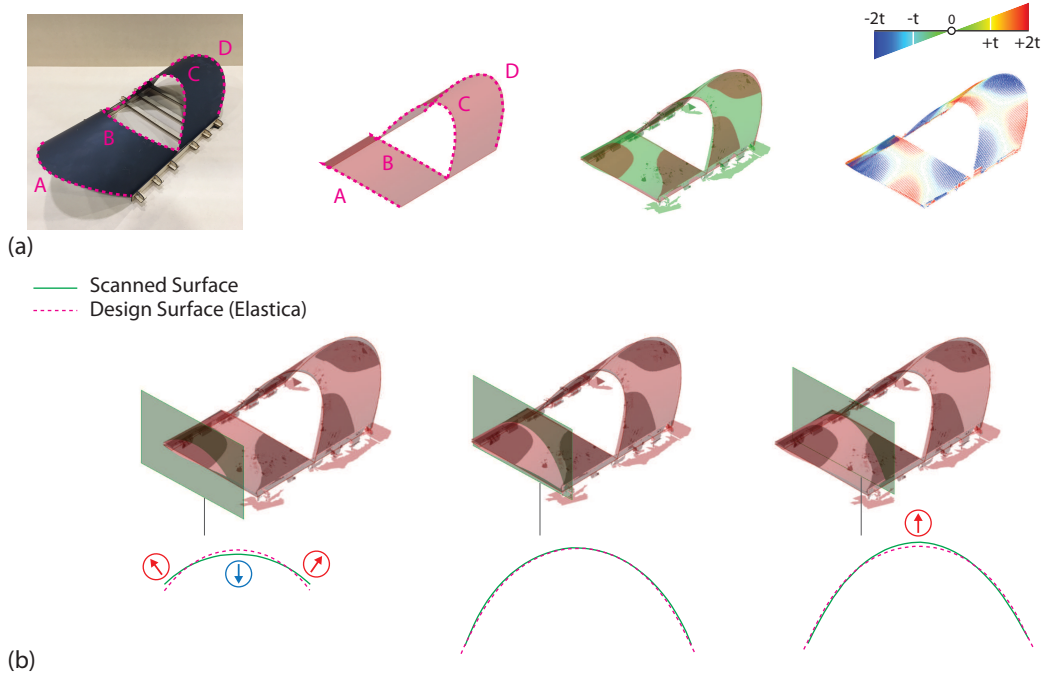


Figure 16: Surface error measurement between elastica generated surface and physical prototype with skewed edges. (a) From left to right: physical prototype, simulated surface, best-fit scanned surface, and surface error measurement result illustration. (b) Cross-sectional comparison.

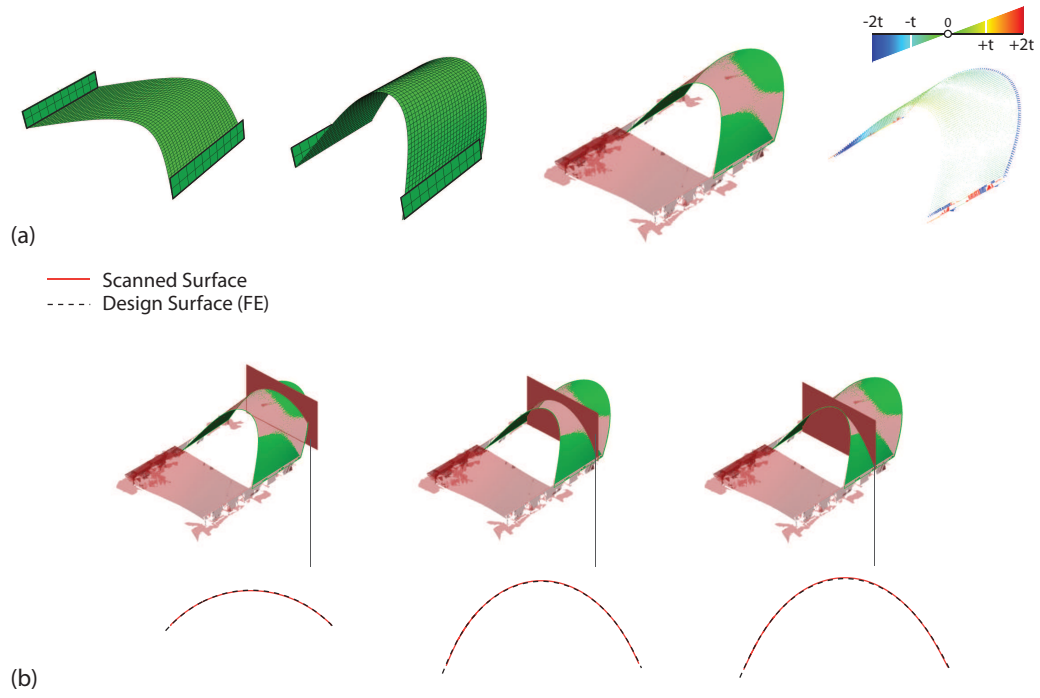


Figure 17: Surface error measurement between finite element simulation and physical prototype with skewed edges. (a) From left to right: undeformed FE model, deformed FE model, best-fit scanned surface and surface error measurement result illustration. (b) Cross-sectional comparison.

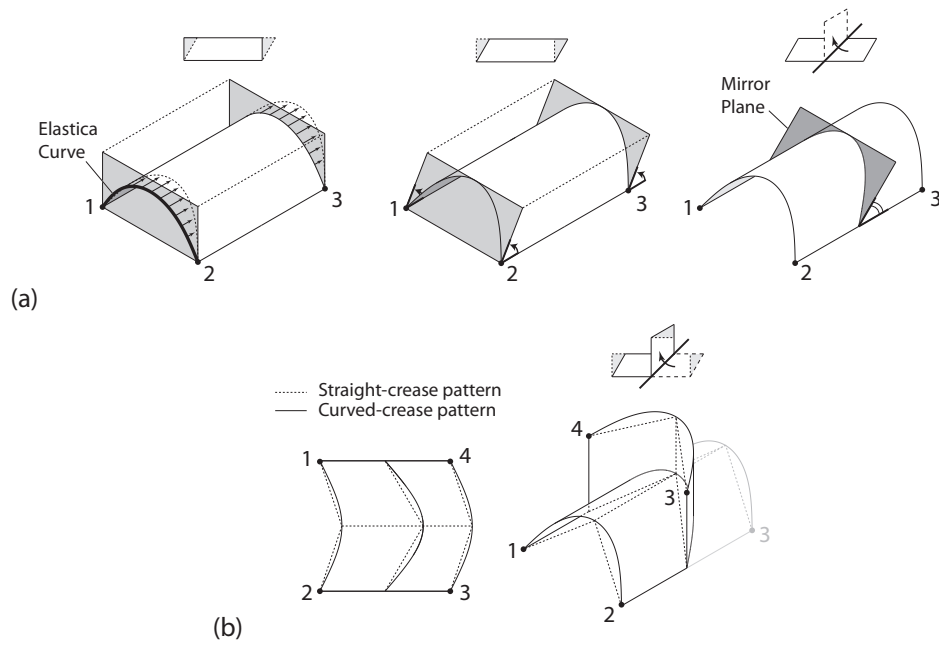


Figure 18: Curved-crease Arc-Miura pattern geometry with skewed free edges. (a) Linear elastica curve extrusion with inclined planes and mirror reflection plane and (b) corresponding unfolded and folded configurations.

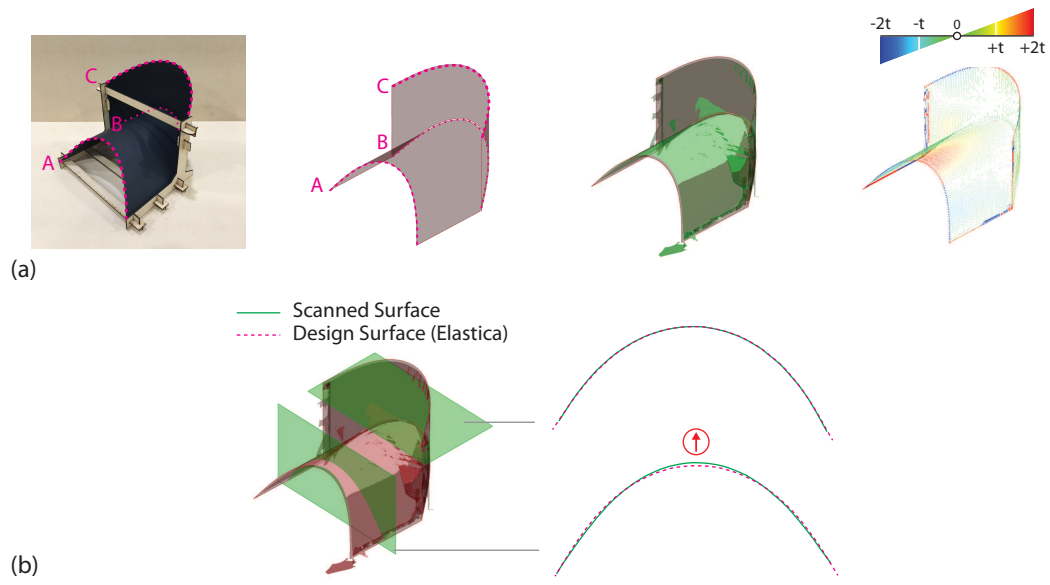


Figure 19: Surface error measurement of single-crease reflection free edge effect. (a) From left to right: physical prototype, simulated surface, best-fit scanned surface, and surface error measurement result illustration. (b) Cross-sectional comparison.

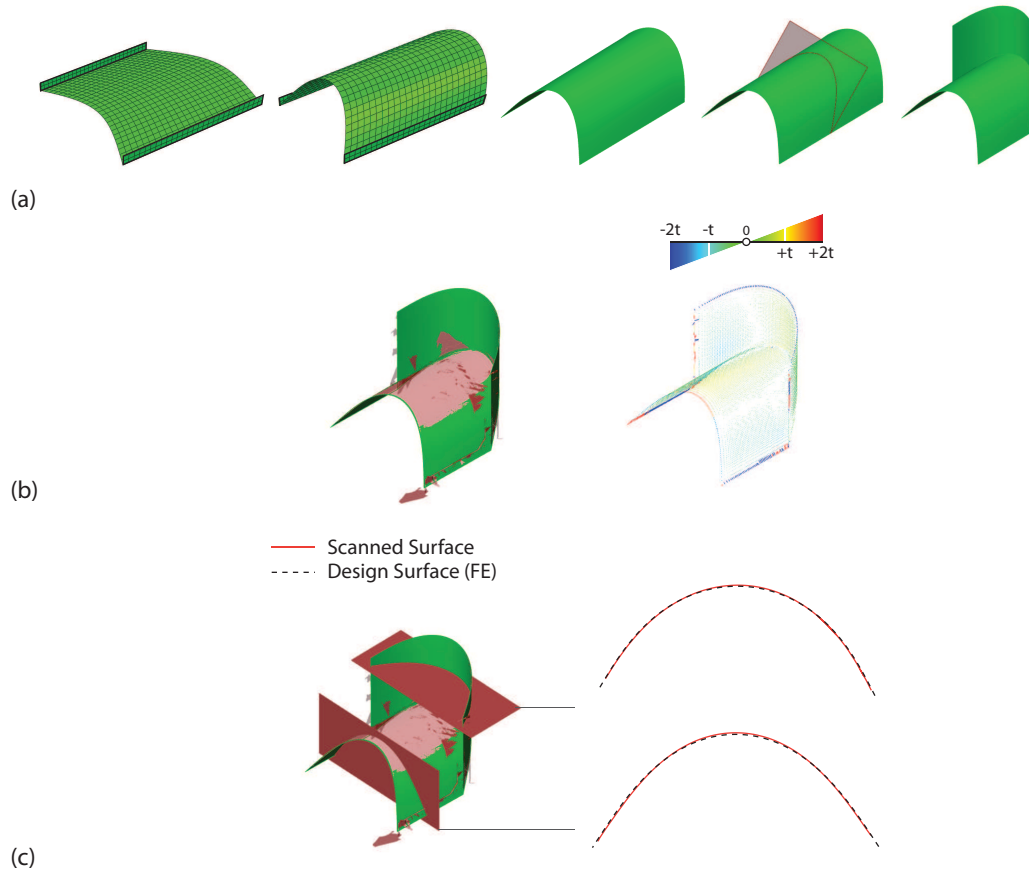


Figure 20: FE simulation of curved-crease origami. (a) Design procedure, from left of right: undeformed FE model, deformed FE model, exported surface, intersecting mirror reflection plane, reflected curved-crease component. (b) Surface error measurement result illustration. (c) Cross-sectional comparison.